npj | quantum materials

Article

Published in partnership with Nanjing University

https://doi.org/10.1038/s41535-026-00848-w

Optical diode effect at telecom wavelengths in a polar magnet

Kevin A. Smith[1], Yanhong Gu[1], Xianghan Xu[2], Heung-Sik Kim[3], Sang-Wook Cheong[2,4], Scott A. Crooker[5] & Janice L. Musfeldt[1,6]

Magnetoelectric multiferroics such as rare earth manganites host nonreciprocal behavior driven by low symmetry, spin-orbit coupling, and toroidal moments, although less has been done to explore whether lanthanides like Er^{3+} might extend functionality into the hard infrared for optical communications purposes. In this work, we reveal nonreciprocity in the *f*-manifold crystal field excitations of *h*-$Lu_{0.9}Er_{0.1}MnO_3$. In addition to contrast in the highest fields, we demonstrate nonreciprocity at technologically-relevant energy scales--specifically in the E-, S-, and C-bands of the telecom wavelength range--and at low magnetic fields and room temperature. In fact, the low field behavior is consistent with possible altermagnetism. These findings advance the overall understanding of localized excitations in rare earth-containing systems and pave the way for entirely new types of telecom applications.

Nonreciprocal directional dichroism is a type of asymmetric light absorption that depends upon propagation direction[1,2]. It is a defining feature of materials that simultaneously break spatial inversion and time-reversal symmetries[3,4]. Although discovered in magnetoelectrics including CuB_2O_4[5–8], $FeZnMo_3O_8$[9], $LiNiPO_4$[10], $LiCoPO_4$[11], $Nd_2Ti_2O_7$[12], $Pb(TiO)Cu_4(PO_4)_4$[13], and Ni_3TeO_6[14–16], nonrecprocity is under-explored in rare earth-containing systems. This is because *f*-manifold crystal field excitations (which are both spin- and parity-forbidden) have been presumed not to host large nonreciprocal effects even though mixing of electric and magnetic dipoles at noncentrosymmetric rare earth sites can generate significant magnetoelectric coupling[1,17]. Properties arising from Er^{3+} are especially relevant to amplifiers, isolators, modulators, and rectifiers at optical communications wavelengths[18–27]. The prospect of integrating additional functionality in the form of nonreciprocity to the rare earth excitations that power these telecommunications technologies is therefore both challenging and potentially transformative. Rather than testing drawn quartz fibers sprinkled with powdered Er[22,23], we employed *h*-$Lu_{0.9}Er_{0.1}MnO_3$ as a platform for examining whether rare earth *f*-manifold excitations have the potential to host nonreciprocal behavior in the hard infrared. This system sports a dilute ensemble of Er^{3+} ions within a $P6_3mc$ matrix that combines spontaneous polarization along *c* (arising from improper ferroelectricity involving the Mn centers) with antiferromagnetism due to Mn^{3+} ordering ($T_N \approx 80$ K) and a rare earth-related transition near 30 K (Fig. 1a)[28,29]. In fact, *h*-$Lu_{0.9}Er_{0.1}MnO_3$ is likely an altermagnet due to antisymmetric spin splitting in the $6'mm'$ magnetic ground state[30]. Our work is enabled by the development of monopolar domain single crystals, which grow in a characteristic canopy-like shape (Fig. 1b). Such a material—if functioning as a secure communications element—should host higher fidelity and lower loss than glass fibers with Er randomly distributed throughout.

The symmetry requirements for toroidal nonreciprocity in *h*-$Lu_{0.9}Er_{0.1}MnO_3$ dictate that polarization, magnetic field, and light propagation direction must be mutually orthogonal[1,4,16]. We therefore performed magneto-optical spectroscopy in this fashion. Strikingly, these measurements reveal strong nonreciprocal behavior in the *f*-manifold crystal field excitations of Er^{3+} that persists not only at high fields but also at modest magnetic fields and even up to room temperature. At 1525 nm, we find a contrast of 3.2% at 1.2 T and 296 K. These findings challenge the conventional wisdom about localized excitations, opening the door to entirely new types of nonreciprocal behavior and applications.

Results and discussion

Er^{3+} crystal field excitations in the hard infrared

Figure 1c, d displays the near infrared absorption of *h*-$Lu_{0.9}Er_{0.1}MnO_3$ as a function of temperature. This particular wavelength range focuses on the Er^{3+} *f*-manifold crystal field excitations in the E-, S-, and C-bands of the telecom range. These excitations are well-known to be sharp and highly localized. The clusters of peaks between 1440 and 1540 nm can be assigned as ${}^4I_{15/2} \rightarrow {}^4I_{13/2}$. This set of excitations is well-studied in Er-containing

[1]Department of Chemistry, University of Tennessee, Knoxville, TN, USA. [2]Department of Physics and Astronomy, Rutgers University, Piscataway, NJ, USA. [3]Department of Semiconductor Physics and Institute of Quantum Convergence Technology, Kangwon National University, Chuncheon, Republic of Korea. [4]Keck Center for Quantum Magnetism, Rutgers University, Piscataway, NJ, USA. [5]National High Magnetic Field Laboratory, Los Alamos, NM, USA. [6]Department of Physics and Astronomy, University of Tennessee, Knoxville, TN, USA. e-mail: musfeldt@tennessee.edu

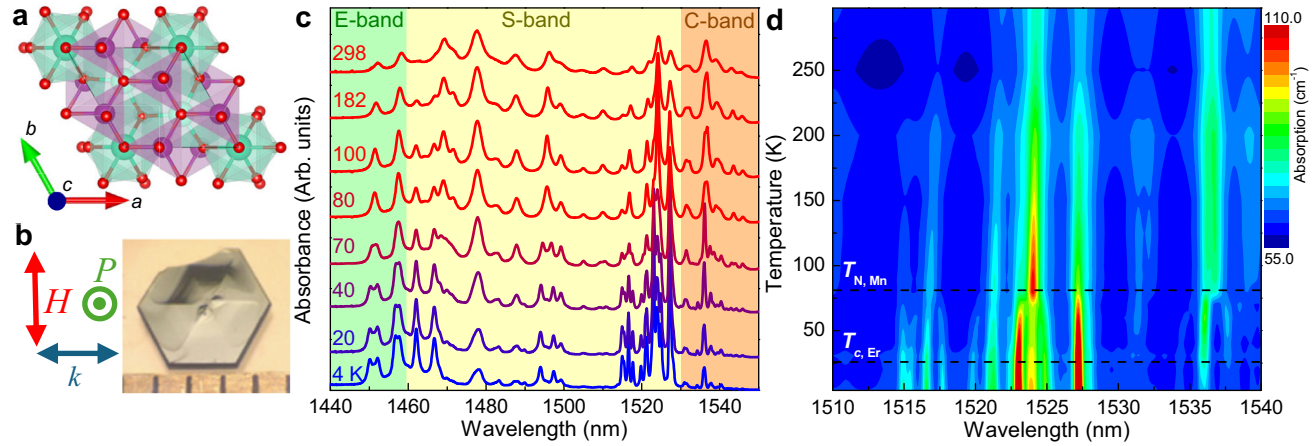

Fig. 1 | Structure, measurement conditions, and temperature effects in *h*-$Lu_{0.9}Er_{0.1}MnO_3$. **a** Crystal structure of *h*-$Lu_{0.9}Er_{0.1}MnO_3$ in the $P6_3mc$ space group[41]. The Lu/Er, Mn, and O sites are indicated by teal, magenta, and red spheres, respectively. **b** Schematic of the measurement geometry indicating the light propagation *k*, applied field *H*, and polarization *P* directions (left) and optical microscope image (right) of the *ab*-plane of the single crystal revealing the natural canopy-like structure that is indicative of a monopolar domain sample. Our single crystals were polished to expose the *c*-axis (which is the direction of polarization) as well as the $\perp c$ direction. Additional information about the orientation (Fig. S1), monopolar domain character (Fig. S5), and magnetic properties (Fig. S6) is provided in the Supplementary Information. **c** Absorption of the $^4I_{15/2} \rightarrow {}^4I_{13/2}$ rare earth crystal field excitations in *h*-$Lu_{0.9}Er_{0.1}MnO_3$ as a function of temperature with the corresponding telecom wavelength ranges indicated in green (E-band), yellow (S-band), and orange (C-band). The spectra are offset for clarity. **d** Contour plot of the spectra in **c** with focus on the S- and C-band features. The horizontal lines indicate Mn^{3+} antiferromagnetic ordering and the Er^{3+}-related transition.

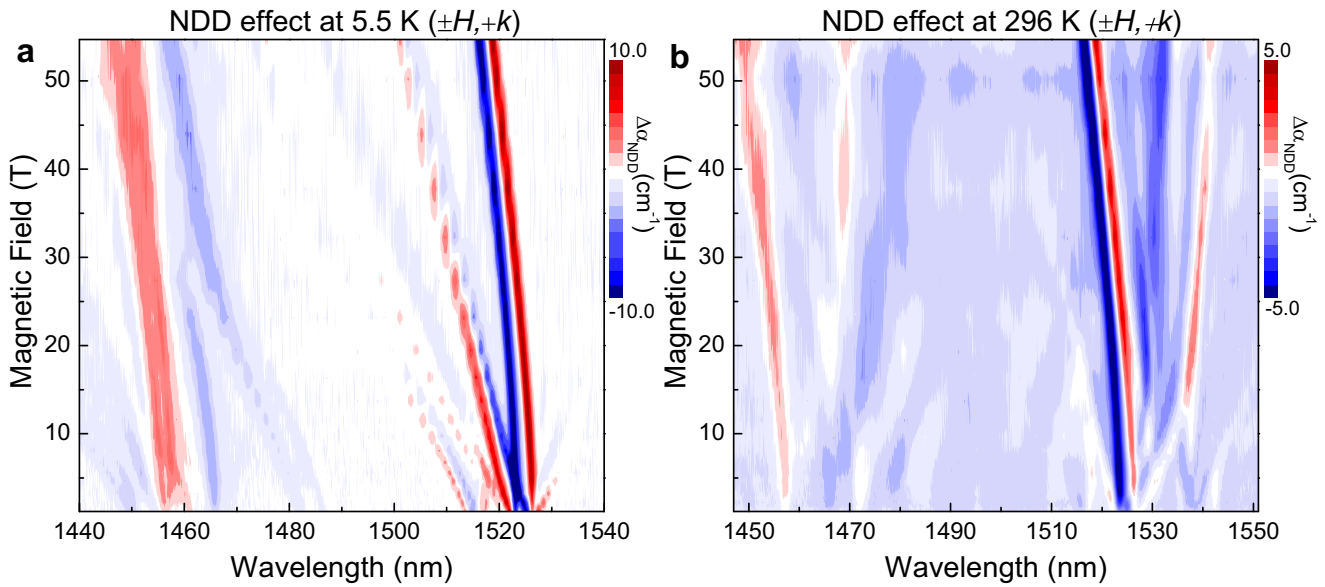

Fig. 2 | Color contour plots of dichroic effects. Nonreciprocal directional dichroism of *h*-$Lu_{0.9}Er_{0.1}MnO_3$ at **a** 5.5 K and **b** room temperature (296 K) in a toroidal geometry in pulsed magnetic fields to 55 T and shown as contour plots. The color indicates the strength and sign of the dichroic signal. Nonreciprocal directional dichroism $\Delta\alpha_{NDD}$ is calculated as $\Delta\alpha_{NDD} = \alpha(+H,+k) - \alpha(-H,+k)$. This quantity is the difference between field pairs.

oxides, chalcogenides, and silica glasses[20–25,31] because the excitations are responsible for the substantial gain near 1550 nm in Er-doped fiber amplifiers for long-range optical communication. *h*-$Lu_{0.9}Er_{0.1}MnO_3$ contains two unique Er^{3+} centers, each with seven primary $^4I_{15/2} \rightarrow {}^4I_{13/2}$ excitations at base temperature, with additional features arising from temperature-induced population effects. The two Er^{3+} sites and the combination of both *ab*-plane and *c*-oriented excitations add to the complexity of the 4 K data. The impact of population effects along with the Er^{3+}-related and Mn^{3+} magnetic ordering transition is evident in the contour plot as well[30,32].

Nonreciprocity in *f*-manifold crystal field excitations

In order to explore how low symmetry and spin-orbit coupling impact the properties of *f*-manifold crystal field excitations, we measured the magneto-optical response of *h*-$Lu_{0.9}Er_{0.1}MnO_3$ at base and room temperatures and calculated the nonreciprocity, which is defined as $\Delta\alpha_{NDD} = \alpha(+H,+k) - \alpha(-H,+k)$. Figure 2 summarizes these results in the form of contour plots. As anticipated, the excitations shift linearly in the magnetic field with different slopes given by the respective *g* factors. We find features that cross and merge as well as excitations that host avoided crossings. The latter defines critical fields at 6 and 30 T, in line with the magnetization of *h*-$ErMnO_3$[30,32] as well as our own measurements of *h*-$Lu_{0.9}Er_{0.1}MnO_3$ (Fig. S6, Supplementary Information). The key point is that nonreciprocity is observed at both low fields and high temperatures and is sensitive to the development of different field-induced magnetic states.

Figure 3 summarizes the dichroic spectra of *h*-$Lu_{0.9}Er_{0.1}MnO_3$. These data were taken in the toroidal configuration with $\pm H$, which is symmetrically equivalent to $\pm k$ (Fig. S2, Supplementary Information)[33]. As a reminder, toroidal dichroism occurs when light propagation is along the

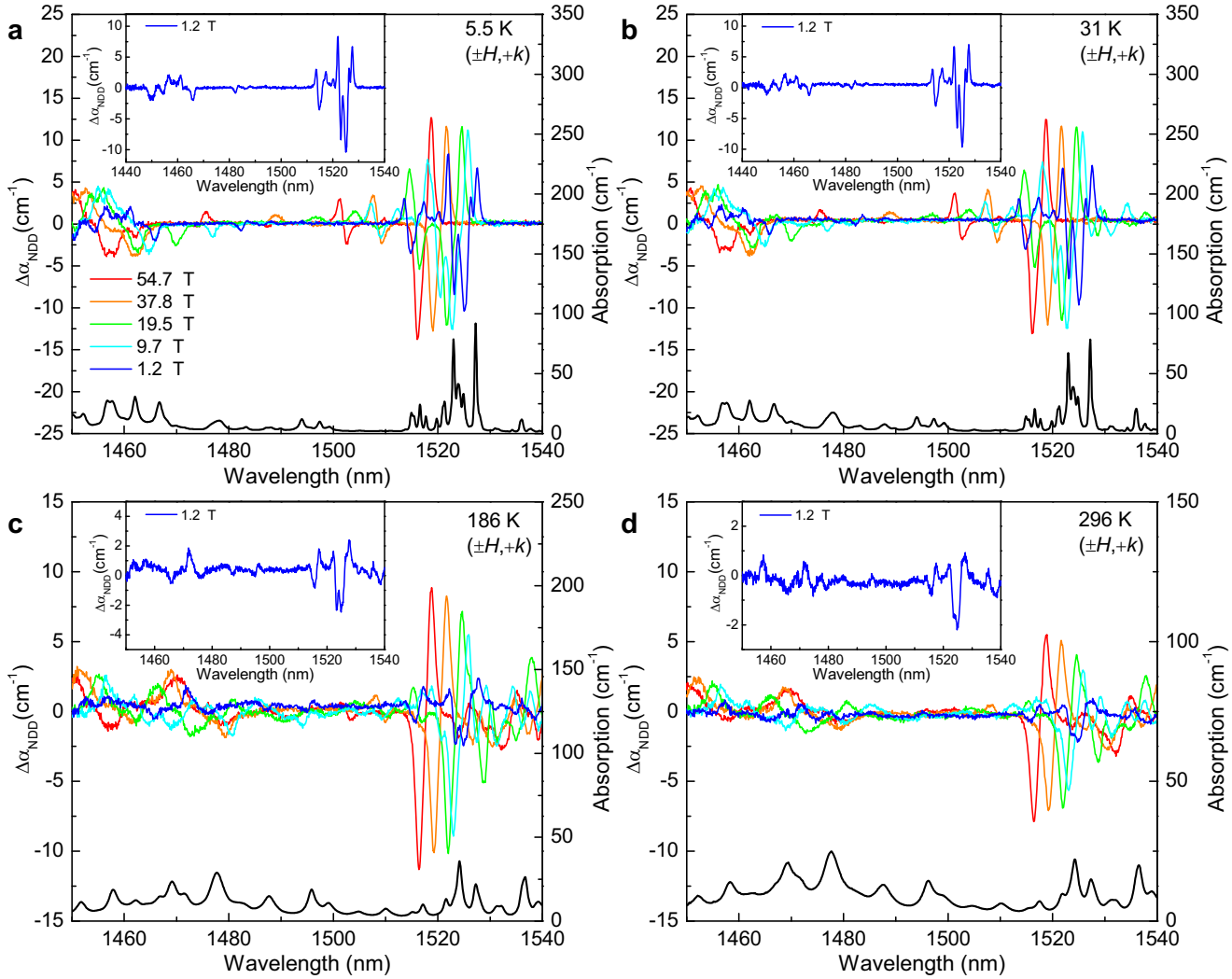

Fig. 3 | Temperature dependence of nonreciprocal directional dichroism. Nonreciprocal directional dichroism of h-$Lu_{0.9}Er_{0.1}MnO_3$ at **a** 5.5 K, **b** 31 K, **c** 186 K, and **d** 296 K at selected fields. The absolute absorption at each temperature is at the bottom of each panel for comparison. These features are assigned as $Er^{3+}{}^4I_{15/2} \rightarrow {}^4I_{13/2}$ crystal field excitations. The insets show $\Delta\alpha_{NDD}$ at 1.2 T.

toroidal moment T ($k \parallel T = P \times M$, where P and M are the electric polarization and magnetic moment)[3,34–38]. We polished and mounted our crystal consistent with this configuration (Fig. S1, Supplementary Information).

Figure 3a displays the nonreciprocal directional dichroism of h-$Lu_{0.9}Er_{0.1}MnO_3$ at 5.5 K, well below the Er^{3+}-related transition and magnetic ordering temperature of Mn^{3+}. The dichroic response is unexpectedly large (18.8% at 1516 nm and 55 T) for such a highly localized set of excitations. These results unequivocally confirm that f-manifold crystal field excitations in a magnetoelectric material can host nonreciprocity. The effect is sharp and clear, with a very systematic response as a function of applied magnetic field. Even more remarkably, we find that this system does not need the highest fields to reveal functionality. $\Delta\alpha_{NDD}$ is approximately 10.4% at 1525 nm and 1.2 T. That such a well-defined nonreciprocal effect can be observed in the telecom wavelength range allows us to conceive of a number of unique opportunities.

To test the impact of magnetic ordering on the dichroic effect, we performed similar experiments at elevated temperatures. Figure 3b, c displays the nonreciprocal directional dichroism of h-$Lu_{0.9}Er_{0.1}MnO_3$ at 31 and 186 K, respectively. There is no rare earth ordering at 31 K[30,32], although the Mn^{3+} centers are still magnetically ordered ($T_N \approx 80$ K). Even so, nonreciprocity is surprisingly strong. Increasing the temperature to 186 K eliminates magnetic ordering involving the Mn^{3+} sites as well. The consequence is a substantial decrease in the size of the dichroic signal. The overall shape changes due to population effects as well. Clearly, Er⋯Mn interactions are important—but not essential—for this process.

Nonreciprocity at room temperature

Inspired by the possibility that a well-ordered magnetic state is not required for the development of nonreciprocity in f-manifold crystal field excitations, we measured the magneto-optical properties of h-$Lu_{0.9}Er_{0.1}MnO_3$ at room temperature. As a reminder, nonreciprocal directional dichroism requires magnetoelectric coupling. This is because the magnetoelectric susceptibility $\chi^{me}_{\alpha\beta}$ is proportional to $\langle 0|P_\alpha|n\rangle\langle n|M_\beta|0\rangle$, so both the polarization and magnetization matrix elements must be non-zero[1].

Figure 3d displays the dichroic response of h-$Lu_{0.9}Er_{0.1}MnO_3$ at room temperature. Strikingly, the effect is not quenched due to a lack of long-range magnetic order in the Mn framework. This is because the toroidal configuration does not require magnetic order since $k \parallel T = P \times M$[3,34,36–39]. Examination reveals that $\Delta\alpha_{NDD}$ is still as high as 13.7% at 1516 nm and full field, although the exact magnitude varies depending upon the excitation, and the overall size of the spectral features is much more field sensitive than before. Not only is the signal larger in higher fields, but the highest fields are needed to obtain well-formed peak shapes. This is likely because larger fields are required to overcome thermal fluctuations, align Er moments, and break time-reversal symmetry in the paramagnetic phase above the ordering temperature. Even at 296 K, h-$Lu_{0.9}Er_{0.1}MnO_3$ continues to host

nonreciprocal directional dichroism at very modest fields. $\Delta\alpha_{NDD}$ at 1.2 T, for instance, is still distinct (inset, Fig. 3d). These findings demonstrate that it is indeed possible to realize room temperature nonreciprocity under low field conditions in the telecom range.

Breaking time reversal symmetry in this system

Thus far, we have seen that at low temperatures, where Mn is antiferromagnetically ordered, Er···Mn interactions break time-reversal symmetry to enable nonreciprocity in the *f*-manifold excitations. We speculate that, in the presence of magnetic order, the Mn-induced local exchange fields on the Er moments cooperate with the external field for an enhanced dichroic response. This provides a way to understand the dramatic spectral changes across the Mn ordering temperature. Below the ordering temperature, *h*-$Lu_{0.9}Er_{0.1}MnO_3$ likely exhibits B_2-type symmetry, corresponding to a $6'mm'$ magnetic point group, suggesting the potential for symmetric and antisymmetric spin splitting (S/A-type altermagnetism)[40]. This may provide a possible explanation for the substantial enhancement of the nonreciprocal signal below T_N (Fig. S4, Supplementary Information). At higher temperatures, where Mn is no longer ordered, the applied field acts on the Er moments directly to break time reversal symmetry, the result generating a smaller, yet still appreciable nonreciprocal signature - even at room temperature. These effects are well within the limits of our sensitivity. Due to the low energy scales for *f*-orbital excitations, small external perturbations lead to a remarkably large nonreciprocal response, 3.2% at 1525 nm and 1.2 T, even at room temperature.

To summarize, we report the discovery of nonreciprocity in the rare-earth crystal field excitations of an Er^{3+}-containing oxide across the telecom wavelength range. The effect is surprisingly strong—a finding that we attribute to the ability of the applied field to rotate Er^{3+} moments. At the same time, there is a polar environment around the noncentrosymmetric rare earth ions, leading to the formation of net toroidal moments even in the presence of very small magnetic fields. While there is some sensitivity to magnetic ordering likely due to altermagnetic character below T_N, the toroidal configuration generally supports low-loss nonreciprocity in monopolar crystals of *h*-$Lu_{0.9}Er_{0.1}MnO_3$ at readily accessible fields and temperatures - including room temperature. These findings open the door to the development of structure-property relations as well as low-power devices in this unique application space.

Methods

Single crystal growth

h-$Lu_{0.9}Er_{0.1}MnO_3$ powder was synthesized by sintering a stoichiometric mixture of Lu_2O_3, Er_2O_3, and Mn_2O_3 powders at 1350 °C for 30 h, with two intermediate grindings. For single crystal growth, the synthesized powder was mixed with Bi_2O_3 flux in a molar ratio of 1:10. The mixture was placed in a platinum crucible, heated to 1100 °C for 10 h, then cooled at a rate of 2 °C per hour to 800 °C, followed by rapid cooling at 100 °C per hour to room temperature. The residual flux was removed using dilute hydrochloric acid to isolate *h*-$Lu_{0.9}Er_{0.1}MnO_3$ crystals. Compared to previously reported flux growth methods that yielded multi-ferroelectric-domain crystals, the approach used here incorporates a higher ratio of Bi_2O_3 flux. As a result, crystallization occurred at the surface rather than at the bottom of the crucible. This surface crystallization effectively poled the crystals into a single ferroelectric domain, as confirmed by optical microscope images of the chemically etched surfaces. The crystals were polished to reveal the *c*-axis (since the polar *c*-axis is normal to the large natural growth face) and to obtain a proper optical density for our experiments. In this case, the thickness was 230 μm. This configuration is shown in Fig. S1, Supplementary Information.

Spectroscopic techniques

Spectroscopic measurements at zero magnetic field were performed using a Bruker Equinox 55 Fourier-transform infrared spectrometer across the infrared range from 800 to 2600 nm, more than covering the telecom wavelengths (1260–1625 nm) and the response of the *f*-manifold excitations in that vicinity. Unpolarized light was used for all experiments. The absorption coefficient was calculated as: $\alpha(\lambda) = (-1/d)\ln(\mathcal{T}(\lambda))$, where $\mathcal{T}$ is the measured normalized transmission, and d is the crystal thickness. An open-flow cryostat was used for temperature control.

Magneto-optical measurements

Magneto-optical spectroscopy was performed at cryogenic temperatures using a 65 T pulsed magnet at the National High Magnetic Field Laboratory in Los Alamos, NM. The samples were mounted in the Voigt geometry on a fiber-coupled probe. Two multi-mode optical fibers were used to deliver broadband, unpolarized, white light to the sample and to collect the light transmitted through the sample, respectively. The collected light was dispersed in a 300 mm spectrometer, using a 600 groove/mm grating, and was detected by a 1024-pixel InGaAs array detector. We focused on the E-, S-, and C-bands of the telecom wavelength range (1460–1565 nm), achieving approximately 0.1 nm spectral resolution to capture changes in the sharp *f*-manifold excitations. To test nonreciprocal directional dichroism, the propagation direction of the light ($\pm k$) through the sample was reversed by switching the delivery and collection fibers and also by reversing the direction of the magnetic field ($\pm H$). A comparison is shown in Fig. S2, Supplementary Information. We provide an example of the raw data collected at ±55 T in Fig. S3, Supplementary Information.

Data availability

The datasets generated and/or analyzed during the current study are not publicly available due to active intellectual property considerations, but are available from the corresponding authors upon reasonable request.

Received: 3 July 2025; Accepted: 2 January 2026;
Published online: 16 January 2026

References

1. Kézsmárki, I. et al. One-way transparency of four-coloured spin-wave excitations in multiferroic materials. *Nat. Commun.* **5**, 3203 (2014).
2. Tokura, Y. & Nagaosa, N. Nonreciprocal responses from non-centrosymmetric quantum materials. *Nat. Commun.* **9**, 3740 (2018).
3. Narita, H. et al. Observation of nonreciprocal directional dichroism via electromagnon resonance in a chiral-lattice helimagnet $Ba_4NbFe_3Si_2O_{14}$. *Phys. Rev. B* **94**, 094433 (2016).
4. Cheong, S.-W. & Huang, F.-T. Trompe L'oeil ferromagnetism—magnetic point group analysis. *npj Quantum Mater.* **8**, 73 (2023).
5. Saito, M., Ishikawa, K., Taniguchi, K. & Arima, T. Magnetic control of crystal chirality and the existence of a large magneto-optical dichroism effect in CuB_2O_4. *Phys. Rev. Lett.* **101**, 117402 (2008).
6. Toyoda, S., Abe, N. & Arima, T. Gigantic directional asymmetry of luminescence in multiferroic CuB_2O_4. *Phys. Rev. B* **93**, 201109 (2016).
7. Nikitchenko, A. I. & Pisarev, R. V. Magnetic and antiferromagnetic nonreciprocity of light propagation in magnetoelectric CuB_2O_4. *Phys. Rev. B* **104**, 184108 (2021).
8. Boldyrev, K. N. et al. Nonreciprocity of optical absorption in the magnetoelectric antiferromagnet CuB_2O_4. *Magnetochemistry* **9** https://www.mdpi.com/2312-7481/9/4/95 (2023).
9. Yu, S. et al. High-temperature terahertz optical diode effect without magnetic order in polar $FeZnMo_3O_8$. *Phys. Rev. Lett.* **120**, 037601 (2018).
10. Kimura, K. & Kimura, T. Nonvolatile switching of large nonreciprocal optical absorption at shortwave infrared wavelengths. *Phys. Rev. Lett.* **132**, 036901 (2024).
11. Tóth, B. et al. Imaging antiferromagnetic domains in $LiCoPO_4$ via the optical magnetoelectric effect. *Phys. Rev. B* **110**, L100405 (2024).
12. Shimada, Y., Kiyama, H. & Tokura, Y. Nonreciprocal directional dichroism in ferroelectric $Nd_2Ti_2O_7$. *J. Phys. Soc. Jpn* **77**, 33706 (2008).
13. Katsuyoshi, T. et al. Nonreciprocal directional dichroism in a magnetic-field-induced ferroelectric phase of $Pb(TiO)Cu_4(PO_4)_4$. *J. Phys. Soc. Jpn* **90**, 123701 (2021).
14. Yokosuk, M. O. et al. Nonreciprocal directional dichroism of a chiral magnet in the visible range. *npj Quantum Mater.* **5**, 20 (2020).

15. Sirenko, A. A. et al. Total angular momentum dichroism of the terahertz vortex beams at the antiferromagnetic resonances. *Phys. Rev. Lett.* **126**, 157401 (2021).
16. Park, K. et al. Nonreciprocal directional dichroism at telecom wavelengths. *npj Quantum Mater.* **7**, 38 (2022).
17. Gao, Y. & Xiao, D. Nonreciprocal directional dichroism induced by the quantum metric dipole. *Phys. Rev. Lett.* **122**, 227402 (2019).
18. Tanabe, S. Rare-earth-doped glasses for fiber amplifiers in broadband telecommunication. *C. R. Chim.* **5**, 815–824 (2002).
19. Ulanowski, A., Merkel, B. & Reiserer, A. Spectral multiplexing of telecom emitters with stable transition frequency. *Sci. Adv.* **8**, eabo4538 (2022).
20. Della Valle, F. & Modesti, S. Exchange-excited $f - f$ transitions in the electron-energy-loss spectra of rare-earth metals. *Phys. Rev. B* **40**, 933–941 (1989).
21. Florez, A., Messaddeq, Y., Malta, O. & Aegerter, M. Optical transition probabilities and compositional dependence of Judd-Ofelt parameters of Er^{3+} ions in fluoroindate glass. *J. Alloy. Compd.* **227**, 135–140 (1995).
22. Desurvire, E. Erbium-Doped Fiber Amplifiers: Principles And Applications. (John Wiley & Sons, Inc., 1994).
23. Wang, Q., Dutta, N. K. & Ahrens, R. Spectroscopic properties of Er doped silica glasses. *J. Appl. Phys.* **95**, 4025–4028 (2004).
24. Rao, R. et al. Multi-band luminescence from a rare earth-based two-dimensional material. *Matter* **8**, 101929 (2025).
25. Zhai, Z. & Sahu, J. K. Progress in Er-doped fibers for extended L-band operation of amplifiers. *Opt. Commun.* **578**, 131510 (2025).
26. Xin, F. et al. Observation of extreme nonreciprocal wave amplification from single soliton-soliton collisions. *Phys. Rev. A* **100**, 043816 (2019).
27. Puel, T. O., Turflinger, A. T., Horvath, S. P., Thompson, J. D. & Flatt,, M. E. Enhancement of microwave to optical spin-based quantum transduction via a magnon mode. *Phys. Rev. Research* **7**, 033221 (2025).
28. Palstra, T. T. M. The Magneto-electric Properties of RMnO Compounds. (Springer, Berlin, Heidelberg, 2007). .
29. Xu, L. et al. Strategy for achieving multiferroic E-type magnetic order in orthorhombic manganites $R\mathrm{MnO_3}$ (R = La-Lu). *Phys. Chem. Chem. Phys.* **22**, 4905–4915 (2020).
30. Song, J. D. et al. Magnetization, specific heat, and thermal conductivity of hexagonal $\mathrm{ErMnO_3}$ single crystals. *Phys. Rev. B* **96**, 174425 (2017).
31. Popova, M. N. et al. High-resolution optical spectroscopy and modeling of spectral and magnetic properties of multiferroic $\mathrm{ErFe_3(BO_3)_4}$. *Phys. Rev. B* **101**, 205108 (2020).
32. Yen, F. et al. Magnetic phase diagrams of multiferroic hexagonal $R\mathrm{MnO_3}$ (R = Er, Yb, Tm, and Ho). *J. Mater. Res.* **22**, 2163–2173 (2007).
33. Hlinka, J. Eight types of symmetrically distinct vectorlike physical quantities. *Phys. Rev. Lett.* **113**, 165502 (2014).
34. Rikken, G. L. J. A., Strohm, C. & Wyder, P. Observation of magnetoelectric directional anisotropy. *Phys. Rev. Lett.* **89**, 133005 (2002).
35. Cheong, S.-W., Talbayev, D., Kiryukhin, V. & Saxena, A. Broken symmetries, non-reciprocity, and multiferroicity. *npj Quantum Mater.* **3**, 19 (2018).
36. Bordács, S. et al. Unidirectional terahertz light absorption in the pyroelectric ferrimagnet $\mathrm{CaBaCo_4O_7}$. *Phys. Rev. B* **92**, 214441 (2015).
37. Fishman, R. S. et al. Spin-induced polarizations and nonreciprocal directional dichroism of the room-temperature multiferroic $\mathrm{BiFeO_3}$. *Phys. Rev. B* **92**, 094422 (2015).
38. Ding, Q. et al. Parity-time symmetry in parameter space of polarization. *APL Photonics* **6**, 76102 (2021).
39. Kézsmárki, I. et al. Enhanced directional dichroism of terahertz light in resonance with magnetic excitations of the multiferroic $\mathrm{Ba_2CoGeO_7}$ oxide compound. *Phys. Rev. Lett.* **106**, 057403 (2011).
40. Cheong, S.-W. & Huang, F.-T. Altermagnetism classification. *npj Quantum Mater.* **10**, 38 (2025).
41. Van Aken, B. B., Meetsma, A. & Palstra, T. T. M. Hexagonal $\mathrm{LuMnO_3}$ revisited. *Acta Crystallogr. E* **57**, i101–i103 (2001).

Acknowledgements

Research at the University of Tennessee is supported by Condensed Matter Physics, Division of Materials Research, U. S. National Science Foundation (DMR-2226109). Work at Rutgers is funded by the W. M. Keck Foundation grant to the Keck Center for Quantum Magnetism at Rutgers University. The National High Magnetic Field Laboratory is supported by the National Science Foundation Cooperative Agreement DMR-2128556, the State of Florida, and the U.S. Department of Energy. H.S.K. was supported by the Basic Science Research Program through the National Research Foundation of Korea, funded by the Ministry of Science and ICT [Grant No. NRF-2020R1C1C1005900, RS-2023-00220471].

Author contributions

J.L.M. and S.W.C. designed the study. X.X. grew the crystals under the supervision of S.W.C. K.A.S., S.A.C., and J.L.M. performed the pulsed field magneto-optical spectroscopies. K.A.S. and Y.G. analyzed the data with guidance from J.L.M. K.A.S. and J.L.M. developed the figures and wrote the manuscript. K.A.S., Y.G., X.X., H.S.K., S.W.C., S.A.C., and J.L.M. commented on the text.

Competing interests

Authors K.A.S., Y.G., X.X., H.S.K., S.A.C., and J.L.M. declare no competing interests. Author S.W.C. serves as an editor of this journal and had no role in the peer-review or decision to publish this paper. Author S.W.C. declares no competing interests.

Additional information

Supplementary information The online version contains supplementary material available at https://doi.org/10.1038/s41535-026-00848-w.

Correspondence and requests for materials should be addressed to Janice L. Musfeldt.